PROCEEDINGS — OF — THE ROYAL SOCIETY A

MATHEMATICAL,
PHYSICAL
& ENGINEERING
SCIENCES

The use of acoustic inversion to estimate the bubble size distribution in pipelines

Timothy G. Leighton, Kyungmin Baik and Jian Jiang

References	**This article cites 41 articles, 3 of which can be accessed free** http://rspa.royalsocietypublishing.org/content/468/2145/2461.full.html#ref-list-1
Subject collections	Articles on similar topics can be found in the following collections chemical engineering (14 articles) mechanical engineering (139 articles) power and energy systems (2 articles)
Email alerting service	Receive free email alerts when new articles cite this article - sign up in the box at the top right-hand corner of the article or click **here**

The use of acoustic inversion to estimate the bubble size distribution in pipelines

By Timothy G. Leighton*, Kyungmin Baik and Jian Jiang

Institute of Sound and Vibration Research, University of Southampton, Highfield, Southampton, Hampshire SO17 1BJ, UK

The most popular technique for estimating the gas bubble size distribution (BSD) in liquids is through the inversion of measured attenuation and/or sound speed of a travelling wave. The model inherent in such inversions never exactly matches the conditions of the measurement, and the size of the resulting error (which could well be small in quasi-free field conditions) cannot be quantified if only a free field code exists. Users may be unaware of errors because, with sufficient regularization, such inversions can always be made to produce an answer, the accuracy of which is unknown unless independent (e.g. optical) measurements are made. This study was commissioned to assess the size of this error for the mercury-filled steel pipelines of the target test facility (TTF) of the spallation neutron source at Oak Ridge National Laboratory, TN, USA. Large errors in estimating the BSD (greater than 1000% overcounts/undercounts) are predicted. A new inversion technique appropriate for pipelines such as TTF gives good BSD estimations if the frequency range is sufficiently broad. However, it also shows that implementation of the planned reduction in frequency bandwidth for the TTF bubble sensor would make even this inversion insufficient to obtain an accurate BSD in TTF.

Keywords: bubbles; acoustics; pipelines; neutron spallation

1. Introduction

The purpose of this paper is to devise a method of estimating the number and sizes of gas bubbles in liquid from the measured attenuation and/or phase speeds of a travelling acoustic wave that is suitable for the mercury-filled steel pipes of the target test facility (TTF) of the \$1.4 billion spallation neutron source (SNS) at Oak Ridge National Laboratory (ORNL), TN, USA. A further aim is to use that method to test whether a sensor based on such principles is practical when it emits the frequency range originally designed, and when it emits the narrower but more affordable frequency range enforced by the 2008 global financial crash.

In an inversion (the estimation of a parameter from measurements where there is not a simple one-to-one mapping and a model is required), a basic ideal requirement is that the assumptions of the model used in the inversion

*Author for correspondence (tgl@soton.ac.uk).

match the conditions under which the measurements are made. Strictly speaking, this has never happened for the most widespread technique of measuring bubble populations acoustically, when the bubble size distribution (BSD) is estimated from the measured attenuation and/or sound speed of a travelling wave (Commander & McDonald 1991; Duraiswami *et al.* 1998; Leighton *et al.* 2004). This is because the model used assumes acoustic plane wave propagation in free field (PWFF) conditions (Commander & Prosperetti 1989).

Some other techniques do not require the measurement of attenuation and sound speed of travelling waves in bubbly liquid. Important examples are the increasingly popular resonator technique (Farmer *et al.* 2005) and the impedance tube method of Wilson *et al.* (2005). Both however could be affected by coupling between the liquid and the container walls, and indeed Wilson *et al.* carefully designed their impedance tube to avoid this regime, stating: 'This impedance tube was designed such that when filled with bubble-free water, both the radial component of the plane wave mode and the higher-order mode are negligible and can be ignored…. An inversion scheme that properly accounts for both components of both modes does not exist and for now these elastic waveguide effects have been ignored' (Wilson *et al.* 2005; p. 1898). They later used the lossless model of Lafleur & Shields (1995) to predict the effect of coupling on the phase speed in bubbly water, but could not predict attenuation or invert for the bubble population. Boston University collaborators on ORNL's bubble detection programme attempted to use a mercury-filled, flow-through, stainless steel cylindrical resonator to measure sound speed. Although their system worked well with water (Ormonde *et al.* 2008; Roy *et al.* 2008), they encountered problems with imperfectly wetted steel/mercury boundaries, particularly when bubbles were introduced (R. A. Roy 2012, personal communication).

Given coupling was a concern to Wilson *et al.* when studying propagation in water-filled tube with thick steel walls, it is not surprise that it becomes a dominant feature of propagation in the mercury-filled steel pipes of the TTF at ORNL. The current paper provides an inversion method which included this effect for measurement of attenuation and speed of travelling waves.

The mismatch between model and scenario has not prevented the PWFF inversion being used in the past, since with sufficient regularization it can always be made to generate an answer, and rarely is an independent measurement made to check the correctness of that answer. In some scenarios (e.g. with low bubble concentrations in deep oceans), the departure from PWFF conditions may produce insignificant errors (Vagle & Farmer 1998). However, the petrochemical, cement, food production, ceramic, power, mining and pharmaceutical industries, etc., require methods for measuring bubble populations in liquids in pipelines (Campbell & Mougeot 1999; Iskandrani & Kojasoy 2001; Punurai *et al.* 2006; Yim & Leighton 2010). Here, the error produced in the mismatch between the environment and the PWFF assumption used in the inversion has never been quantified, let alone corrected for. This paper provides these two advances. In §2, simulated data are used, because for this the input bubble population is known and the errors in the inversion are clearly quantified. It is shown that the PWFF inversion produces large errors in the estimation of the BSD (greater than 1000% overcounts/undercounts). A new method of inversion is provided, which takes into account the fact that the measurements were

not made under PWFF conditions but instead occurred in a pipe where coupling occurs between the pipe walls and the fluid inside it. This inversion is validated against simulated data from pipes and is shown to give similar levels of accuracy to those obtained when the PWFF inversion is applied to data taken in PWFF conditions. Section 3 describes experimental tests on water-filled poly methylmethacrylate (PMMA) pipes, which had previously been shown to mimic the acoustic coupling that would occur in the mercury-filled steel pipes of ORNL's SNS TTF (Baik *et al.* 2010; Jiang *et al.* 2011). Although these data show that the new inversion technique would provide accurate BSDs if the frequency range of the original sensor design were to be used, budget cuts forced by the 2008 global financial crisis dramatically reduced the frequency range that could be afforded. Section 4 demonstrates that it is not worth ORNL commissioning a sensor with this reduced frequency range, because although it is affordable, the loss of accuracy is unacceptable.

Measurement of the bubble population is however important for ORNL, since helium bubble injectors are planned to be fitted to the SNS in 2013 to absorb the shocks generated when the proton beam impacts the mercury. Such absorption will mitigate cavitation damage to the casing surrounding the mercury (Chitnis *et al.* 2010; Manzi *et al.* 2010; Leighton *et al.* 2011).

Assessment of the effect of applying PWFF inversions to pipe data, and assessment of the investment which needs to be made to cover enough frequencies to produce satisfactory results, are vital steps if industry is to make use of acoustic inversions for BSD in pipes. This approach should replace the current faith that the technique can produce an answer (as it always can be made to do) without questioning the accuracy of that answer.

The theory underlying the PWFF inversion technique assumes that plane waves propagate, with a single sound speed and known frequency-dependent attenuation in bubble-free conditions. When bubbles are added in PWFF conditions, at any given frequency there exists a single sound speed (which is frequency dependent), and the attenuation changes. These changes are attributed wholly to the presence of bubbles. When modal propagation occurs in pipes where the liquid is coupled to the walls, even in bubble-free conditions each mode propagates with its own frequency-dependent longitudinal phase velocity and attenuation (Baik *et al.* 2010). The differences between these phase speeds and attenuations, and those assumed for infinite volumes of bubble-free liquid, would be attributed by the PWFF inversion as being caused by bubble presence. In such circumstances, if an industry cannot cancel out this error by generating bubble-free conditions and instead relies on a predicted bubble-free attenuation, then use of a PWFF inversion would give a finite bubble count even when no bubbles are present. The errors in the inversion when bubbles are added have not previously been investigated. It should be noted that there are further sources of mismatch that are not included in the formulation of this paper, but which have been considered elsewhere (§4*a*).

The methods developed in this paper have also been used to provide demonstrations for TV, public shows and student demonstrations of the ability of bubbles in liquids, and aerosol drops in air, to absorb sound (Leighton *et al.* 2011, 2012).

2. Theory

(*a*) *The forward problem*

For pipes with boundary conditions resembling those of the mercury-filled steel pipes of ORNL or the water-filled PMMA pipes of §3, Baik *et al.* (2010) showed how the complex axial wavenumber, q'_{0m} of the axisymmetric coupled modes that propagate in the axial direction is obtained by their eqn (6) with the matrix elements of their appendix B (the '0' in the subscript '$0m$' refers to the mode being axisymmetric and 'm' refers to the mode index). Eqn (6) of that paper gives the infinite number of the axisymmetric modes (denoted as ETm where m is mode index related to the radial motion) and the real and the imaginary parts of the complex solution, q'_{0m}, which give the phase speed and the attenuation of the modes respectively in a pipe containing a bubble-free liquid.

The introduction of bubbles into the previously bubble-free liquid in the pipe changes the elastic properties of the liquid. The complex wavenumber k'_1 in the liquid is far more influenced by the bubble-induced changes in compressibility than it is by the changes in the spatially averaged density of the bubbly mixture (at least up to gas volume void fractions of 10%). Changes in the complex wavenumber k'_1 affect both phase speed and attenuation, and bubbles moreover scatter the sound and change the stress elements and displacement vectors in the liquid contacting the inner pipe wall.

The sound velocity of a bubbly liquid in a thin elastic tube has been calculated using a one-dimensional approach and the balance between equations of mass, momentum and energy (Rath 1981; Schubert 1991). The result predicts subsonic sound speeds as a function of the gas volume void fraction, but it is not sufficient for the current study because acoustic coupling between the elastic solid and the bubbly liquid will in practice also give an infinite number of supersonic modes. To encompass such modes in this study, the characteristic equation for the axisymmetric modes in a tube filled with bubbly liquid is implemented by combining the description of acoustic modes in a pipe containing bubble-free liquid (Baik *et al.* 2009, 2010) with an analysis which predicts the bubble-induced changes in phase speed and attenuation that occur in an infinite bubbly liquid (Commander & Prosperetti 1989). Wilson *et al.* (2005) applied the formulation of Commander & Prosperetti (1989) in order to measure the phase speed and attenuation that occurred in an impedance tube made of heavy stainless steel, where the phase speed of the lowest axisymmetric mode at low frequencies does not differ significantly from the intrinsic sound speed of the liquid within the tube. In their approach, the phase speed of the dominant axisymmetric modes in the bubble-free waveguide is used as an input parameter. In contrast, the current study uses the BSD as a parameter to obtain the dominant axisymmetric modes in the bubbly waveguide.

For a given homogeneous size distribution of bubbles in an infinite liquid undergoing steady-state pulsations in the linear long-wavelength limit (Clarke & Leighton 2000; Leighton *et al.* 2004), the complex phase speed of sound in bubbly liquid, C_b, is given, with the $-i\omega t$ convention, by

$$\frac{C_1^2}{C_b^2} = \frac{k'^2_1}{k^2_1} = 1 + 4\pi C_1^2 \int_0^\infty \frac{R_0 n_b(R_0)\mathrm{d}R_0}{\omega_0^2 - \omega^2 - 2ib\omega}, \qquad (2.1)$$

where C_1 is the intrinsic sound speed in bubble-free liquid (Commander & Prosperetti 1989), R_0 is the equilibrium bubble radius, ω_0 is the resonance frequency and b is the total damping parameter (Ainslie & Leighton 2011). The presence of bubbles changes the acoustic impedance of liquid, reducing it at low frequencies in infinite media (Mallock 1910; Leighton & Robb 2008), but tending to increase it at frequencies just above the bubble resonance (Commander & Prosperetti 1989). This change is described by the transformation of the real wavenumber in bubble-free liquid, k_1, into the complex wavenumber in bubbly liquid, k_1'. The BSD is described by $n_b(R_0)$, where $n_b(R_0)\mathrm{d}R_0$ is the number of bubbles per unit volume having radii between R_0 and $R_0 + \mathrm{d}R_0$ (where conventionally $\mathrm{d}R_0 = 1\,\mu\mathrm{m}$ when such populations are represented graphically). The gas volume void fraction, Γ, is given by $\Gamma = 4\pi \int R_0^3 n_b(R_0)\mathrm{d}R_0/3$. The total damping parameter, b, includes b_{th}, b_{vis} and b_{rad}, corresponding to thermal, viscous and radiation damping, respectively, and explicit forms of ω_0 and b are given by Commander & Prosperetti (1989) (those authors, who unlike here write with the $+ j\omega t$ convention, have identified and thoroughly publicized a typographical error in their expression for b_{th}; Ainslie & Leighton 2011). A key assumption is that the complex wavenumber k_1' in equation (2.1) refers to the wavenumber in the infinite body of the bubble-free liquid. This must be adapted for the situation when the bubbly liquid is contained within a tube, where the bubbles change the pressure field within the pipe and, accordingly, the complex wavenumber k_1' also changes. It is assumed that the bubbly liquid axisymmetrically exerts on the tube wall an average pressure which is established by equation (2.1). Therefore, when a bubbly liquid with a known BSD fills an elastic pipe, the axisymmetric modes within the pipe are calculated by substituting the expression of k_1' from equation (2.1) into eqn (6) (with the matrix elements of appendix B) of Baik *et al.* (2010).

This is done in figure 1. The solid curves predict the phase speed (identical solid curves in (a) and (c)) and attenuations (identical solid curves in (b) and (d)) of three modes when the PMMA pipe is filled with bubbly water. The BSD of the bubbly water is based on the smoothed version of the optically measured BSD (the solid black μCORT curve of figure 3), where equation (2.1) in this paper and eqn (6) of Baik *et al.* (2010) are used to predict all the solid curves in (a–d). These are plotted as a function of wavenumber-radius product, $x = k_1 a$, where a is the inner radius of the tube. To show the effect made by the addition of bubbles, the dashed lines in figure 1a,b show the modal phase speeds and attenuations when the same pipe is filled with bubble-free water. To show the effect made by the pipe walls, the dashed lines in figure 1c,d show the modal phase speeds and attenuations for PWFF propagation in an infinite (unconfined) volume of bubbly water with the same BSD (as calculated by equation (2.1)). This clearly indicates the degree of error which would occur if the measured sound speed in a pipe were inverted using PWFF theory to infer BSD, the method currently used in such inversions (Hansen *et al.* 2004). Looking at figure 1a for example, an accurate inversion should be based on this change in the modal speeds caused by the introduction of bubbles. It should *not* be based (as the PWFF inversions would do) on the departure of any curve from the horizontal line given by $C_{0m}/C_1 = 1$, an approach made worse when the 'time of first arrival' is used to calculate sound speed (without recognizing modal propagation) as this selects data for the faster modes.
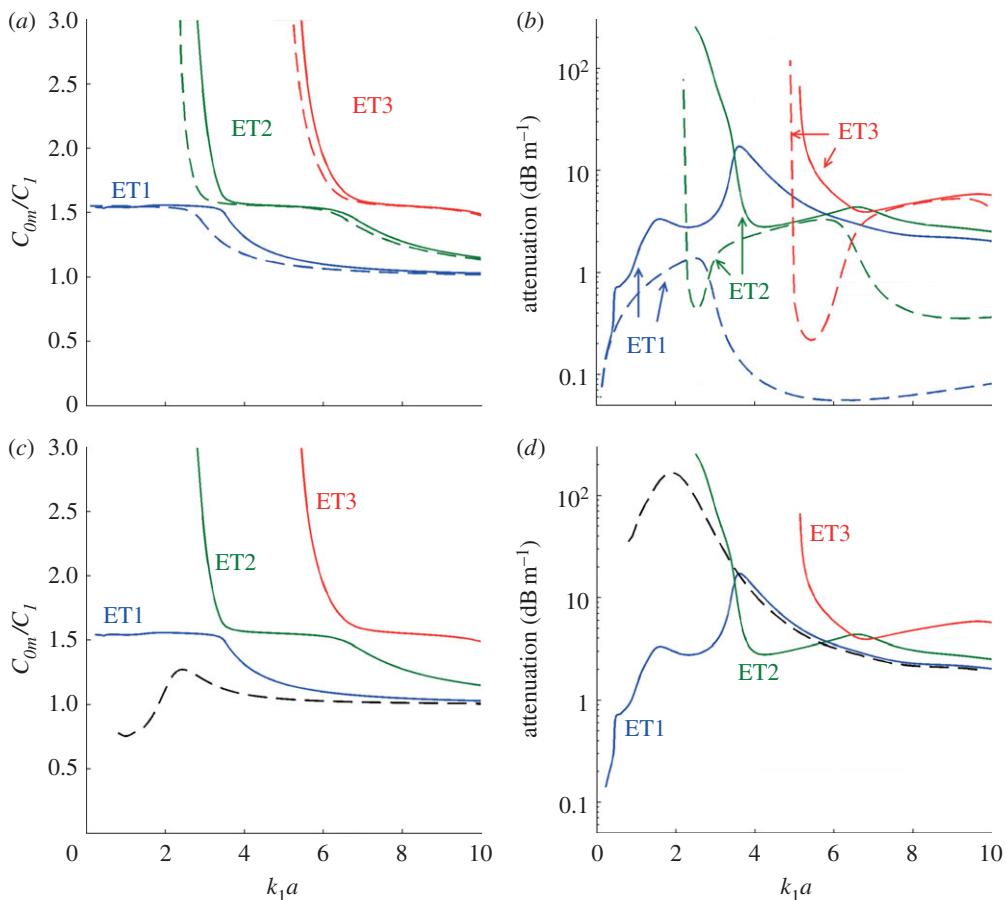
Figure 1. Solid lines show the modal phase speeds (solid lines in (a), identical in (c)) and attenuations (solid lines in (b), identical in (d)) in the PMMA tube filled with bubbly water. The dashed lines in (a,b) show the effect of removing the bubbles from the tube. The dashed lines in (c,d) show the phase speed and attenuation for PWFF propagation in an infinite volume of bubbly water, unconfined by the tube. All BSD's are based on the solid black line of figure 3. (Online version in colour.)

If the only measurements available were the dispersion relation of the modes with (solid curves in (a) and (b)) and without (dashed curves in (a) and (b)) bubbles present, could the BSD be inferred uniquely? The two sets of dispersion curves are sufficiently similar to allow identification of features, but the question is whether these features change sufficiently to act as a good indicator of BSD directly. For example, the break points (Baik $et\ al.$ 2010) where two modes come into closest approach (barring the tendency to converge as $x \rightarrow \infty$) occur in bubble-free conditions at $x \sim 2.8$ for ET1 and ET2, and $x \sim 6.4$ for ET2 and ET3. When this BSD is introduced, these break points shift to slightly higher frequencies. Another potential indicator is that the phase speeds of the supersonic modes in the bubbly pipeline are higher than those in bubble-free conditions over most of the frequency range shown.

Figure 1*b* shows that throughout most of this frequency range in the pipe, for this BSD the attenuation of a given mode in bubbly water is larger than that in the bubble-free case. This might be expected from the high absorption per metre seen in infinite volumes of bubbly liquid (shown for convenience using the dashed curves in figure 1*d*). It is interesting to note that for ET1 the attenuation rate in the pipe is less (e.g. in the frequency range of $x < 4$) than for plane waves in an infinite body of water for the same BSD as shown in figure 1*d*. The reason for this is that the longitudinal and the shear ultrasonic absorptions in the PMMA are less than the absorption in free field bulk bubbly water in that frequency range. As a result, the acoustic coupling between bubbly water and the PMMA results in the intermediate attenuation of the ET1 mode between the absorptions of the PMMA and bubbly water.

In summary, it is important to note that the significant discrepancy between the phase speeds and attenuation for plane waves in an infinite body of liquid (the dashed curves in figure 1*c,d*) and the values predicted for the same BSD contained within the pipe (solid lines) means that inversions that apply the standard methods (Commander & McDonald 1991; Duraiswami *et al.* 1998) to bubbly water contained in vessels will generate errors in the inferred BSD.

(*b*) *The inverse problem*

It is now routine to compare the attenuation measured across a wide range of frequencies between two hydrophones before and after the injection of bubbles to infer the bubble population through inversion in conditions of low void fraction (Commander & McDonald 1991). Although in principle this can also be done for phase speed (Duraiswami *et al.* 1998), in practice, this is not so useful, since small changes in phase calibration of the hydrophones, or displacements or inaccuracies in hydrophone position, can give large artefacts, and at the very least good practice would require that the measurement be repeated with the hydrophone positions swapped to an accuracy very much less than the smallest wavelength used.

Even if used in actual PWFF conditions, there are complications with such inversions: for example, the algorithms assume no bubbles exist that are resonant outside of the bandwidth of insonification, so that attenuation caused by any bubbles that occur in these two forbidden size regions must be accounted for by erroneously enhancing the bubble count within the allowed bandwidth. An iterative approach to estimating the BSD can be undertaken to mitigate this effect, but this is rarely done (Caruthers *et al.* 1999). Most importantly, with sufficient regularization almost any measured attenuation could be inverted to give an estimated BSD, but there is no in-built validation that this estimate of the BSD is accurate. This can be illustrated by the way in which changes to the regularization can yield different estimates of the BSD for the same input data. Hence provision of an answer from this method does not indicate that it is the correct answer.

Assume that the liquid is effectively infinite and homogeneous, that the void fraction is $\ll \sim 0.0001$ unless multiple bubble–bubble interactions are taken into account (Kargl 2002) and that all bubbles are spherical and pulsate linearly in the steady state (Clarke & Leighton 2000). If the perturbations in the radius of the oscillating bubble, ΔR, are small (i.e. $\Delta R \ll R_0$), then from equation (2.1)

the real and imaginary parts of the squared complex wavenumber, $k_1'^2$, can be respectively approximated as follows

$$
\left.
\begin{aligned}
u_\psi^2 - v_\psi^2 &\approx 1 + 4\pi C_1^2 \Delta R_0 \sum_{\xi=1}^{M} \frac{(\omega_{0\psi\xi}^2 - \omega_\psi^2)R_{0\xi}}{(\omega_{0\psi\xi}^2 - \omega_\psi^2)^2 + 4b_{\psi\xi}^2\omega_\psi^2} n_{\mathrm{b}}(R_{0\xi}) \\
u_\psi v_\psi &\approx 4\pi C_1^2 \Delta R_0 \sum_{\xi=1}^{M} \frac{b_{\psi\xi}\omega_\psi R_{0\xi}}{(\omega_{0\psi\xi}^2 - \omega_\psi^2)^2 + 4b_{\psi\xi}^2\omega_\psi^2} n_{\mathrm{b}}(R_{0\xi}),
\end{aligned}
\right\}
\tag{2.2}
$$

and

where $u_\psi = \mathrm{Re}[k_1']/k_1$ and $v_\psi = \mathrm{Im}[k_1']/k_1$ are the ψth elements of the normalized real and imaginary parts of the complex wavenumber k_1'. The subscripts ξ and ψ are necessary in the statement of $\omega_{0\psi\xi}$ because of the dependence of the resonance frequency in the matrix element on the driving frequency through the frequency dependence of the polytropic index (Ainslie & Leighton 2011). Because M is the total number of discretized elements in the implementation of equation (2.2), the sampling interval of bubble radius ΔR_0 is related to M by $\Delta R_0 = (R_2 - R_1)/(M-1)$ where R_1 and R_2 are the minimum and maximum equilibrium radii contained in the bubble distribution. Equation (2.2) shows how u_ψ and v_ψ are related to each other for a given frequency element ω_ψ. Stacking equation (2.2) along a frequency range of $[\omega_1, \omega_2]$ (where ω_1 and ω_2 are minimum and maximum frequencies in the measurement) recasts equation (2.2) into the following matrix form:

$$
\mathbf{Z}\mathbf{N_b} = \mathbf{1},
\tag{2.3}
$$

the matrix $\mathbf{1}$ is a $N \times 1$ matrix representing unity throughout a given frequency element ω_ψ, and $\mathbf{N_b}$ is a $M \times 1$ matrix of which each element is the bubble size spectrum $n_{\mathrm{b}}(R_{0\xi})$ at a given equilibrium radius of bubble, $R_{0\psi}$. The matrix $\mathbf{Z}$ has a dimension of $N \times M$ and each element $Z_{\psi\xi}$ can be represented as

$$
Z_{\psi\xi} = \frac{4\pi C_1^2 \Delta R_0 R_{0\xi}}{(\omega_{0\psi\xi}^2 - \omega_\psi^2)^2 + 4b_{\psi\xi}^2\omega_\psi^2} \left[\left(\frac{1}{Y_\psi} - Y_\psi\right) b_{\psi\xi}\omega_\psi - (\omega_{0\psi\xi}^2 - \omega_\psi^2) \right],
\tag{2.4}
$$

where $Y_\psi = v_\psi/u_\psi$ is the ratio of the imaginary part to the real part of the complex wavenumber k_1'. The bubble resonance frequency, ω_0, and total damping parameter, b, are also functions of ω_ψ and $R_{0\xi}$ (Ainslie & Leighton 2011). Equation (2.4) requires knowledge of both the phase speed change and the attenuation caused by bubbles in order to estimate the BSD, $\mathbf{N_b}$. Such knowledge is provided by the measurement of $Y_\psi = v_\psi/u_\psi$ in the formulation. The conventional acoustic inversion problem (which only requires measurement of the attenuation) is reconstructed when only the term associated with $1/Y_\psi$ inside the square bracket of equation (2.4) is considered, and the condition of $\mathrm{Re}[k_1'] = k_1$ is imposed. Estimation of the measured BSD, $\mathbf{N_b}$, from the attenuation ($\boldsymbol{\alpha}$) that was measured across a sufficiently wide frequency range (i.e. one that encompasses the pulsation resonances of all bubbles present) is a problem of linear algebra that is an *ill-posed* inversion requiring regularization (Tikhonov & Arsenin 1977; Commander & McDonald 1991; Hansen 1998; Leighton *et al.* 2004). The current study uses Tikhonov regularization (Tikhonov & Arsenin 1977; Hansen 1998), which requires the user to define a regularization parameter close to the optimal value. In order to find the optimal value, the current study

adopted the L-curve method which finds the vertex of the curve that plots the Euclidian norm of the regularized solution against the norm of the error (Leighton *et al.* 2004).

As stated in §2*a*, PWFF theory assumes that there exists a single frequency-dependent attenuation, and a single sound speed that is frequency-independent in the bubble-free condition and frequency-dependent when bubbles are added. However, in pipelines both sound speed and attenuation are multi-valued at any given frequency and are functions of frequency in both bubbly and bubble-free conditions. The two sets of observations cannot match over a broad frequency range, as was shown by the mismatch between the dashed and solid lines in figure 1*c,d*. Application of equation (2.3) to invert attenuation to estimate BSD in pipelines would be erroneous. There are further sources of mismatch that are not considered by this paper (§4*a*).

In order to invert the complex wavenumber measured in a bubbly pipeline to estimate the BSD, this paper develops a technique based on estimating the complex wavenumber that would occur in the infinite body of bubbly liquid that had the same BSD as was present inside the pipeline. This is achieved by applying a Taylor expansion to the formulation of the forward problem described in §2*a*. For a given complex wavenumber (k_1') in the liquid contained inside the tube, the complex wavenumber of the propagating mode inside the tube, q_{0m}' (the real part of which is used to calculate C_{0m}) satisfies the following equation:

$$F(k_1', q_{0m}') = 0, \tag{2.5}$$

where F appears in Baik *et al.* (2010) as the left-hand side of their eqn (6) with the matrix elements in their appendix B. Let the complex wavenumbers in the infinite body of bubble-free liquid and bubbly liquid be k_{1f}' and k_{1b}', respectively (where the infinite bubbly liquid has the same BSD as is occurring in the pipe). Let the complex wavenumbers of the axisymmetric modes in the bubble-free liquid and bubbly liquid inside the pipe be q_{0mf}' and q_{0mb}', respectively. Suppose that the phase speed and the attenuation are measured in the pipe when it is filled with the bubbly liquid. This measurement gives q_{0mb}'. The complex wavenumbers, k_{1f}' and q_{0mf}', can be measured, although it is safest to check that nominally bubble-free measurements agree with the truly bubble-free predictions of Baik *et al.* (2010) in cases where, as in TTF, the convoluted sealed pipework has a history of previous injection of barely soluble gas. The only unknown variable is the complex wavenumber, k_{1b}', which is the input parameter in the acoustic inversion problem to estimate the BSD. This is obtained from the following step. The variables, k_{1f}', k_{1b}', q_{0mf}' and q_{0mb}' should satisfy equation (2.5), that is:

$$F(k_{1f}', q_{0mf}') = 0 \tag{2.6}$$

and

$$F(k_{1b}', q_{0mb}') = 0. \tag{2.7}$$

Provided that the introduction of bubbles inside the pipe does not change phase speed and the attenuation of the modes much from those in bubble-free liquid

such that $|q'_{0mb}/q'_{0mf} - 1| \ll 1$ (figure 1), then equation (2.7) can be expanded to the first order by Taylor expansion:

$$F(k'_{1b}, q'_{0mb}) \approx F(k'_{1f}, q'_{0mf}) + \left[\frac{\partial F(k'_1, q'_{0m})}{\partial k'_1} \Delta k'_1 + \frac{\partial F(k'_1, q'_{0m})}{\partial q'_{0m}} \Delta q'_{0m} \right]. \qquad (2.8)$$

The current study adopted the model by Commander & Prosperetti (1989) to describe the complex wavenumber in a bubbly liquid that was developed from the linearized Keller equation. We assume that the small deviation between axial wavenumbers in bubble-free liquid and in bubbly liquids is linear, allowing use of a Taylor expansion to map from one to the other. Although the choice of a linear method imposes technique-sensitive limitations, it has the advantage over other options (such as use of Bayesian statistics) in the situation where measurements are only possible over certain limited frequency regimes. In such circumstances, the probability distribution (defined in terms of frequency or number of modes) does not change smoothly, generating discontinuities in the probability distribution.

From equations (2.6)–(2.8), the changes in the complex wavenumber in liquid are

$$\Delta k'_1 = -\Delta q'_{0m} \left[\frac{\partial F(k'_1, q'_{0m})/\partial q'_{0m}}{\partial F(k'_1, q'_{0m})/\partial k'_1} \right] \{k'_1 \rightarrow k'_{1f}, q'_{0m} \rightarrow q'_{0mf}\}. \qquad (2.9)$$

Therefore, k'_{1b} is estimated to be $k'_{1f} + \Delta k'_1$, and this is used as an input parameter of the acoustic inversion described in equation (2.3). The bubble-free and bubbly conditions inside the tube are accounted for by $\Delta q'_{0m}$ which contains the change of phase speed and additional damping.

Numerical error is always a problem when equation (2.9) is applied to an inverse problem to estimate the BSD contained in the pipe. Such errors contain values of k'_{1b} which are either too small or too large. In the worst case, the value of k'_{1b} estimated through equation (2.9) generates negative values, which will be shown in figure 4a. These numerical errors come from steep changes of derivatives of the characteristic equation $F(k'_1, q'_{0m})$ with respect to change of q'_{0m} or k'_1. Sometimes, it changes phase, and therefore negative elements of the wavenumber can be obtained within the linear variances of q'_{0m} and k'_1. Of course such errors can be mitigated by expanding the Taylor series to higher order. However, this makes the estimation of k'_{1b} more complicated, and even with higher-ordered expansions, such numerical errors still exist whenever large changes between bubbly and non-bubbly conditions are observed. Therefore, in the actual implementation of equation (2.9), limitations of the range of $\Delta k'_1$ are imposed so that if the resulting estimate of k'_{1b} were to be too large or too small, it is abandoned and q'_{0mb} is used in its place. It is apparent in figure 1 that the differences between the imaginary parts (corresponding to the attenuation) of k'_{1b} (for an infinite volume of bubbly water) and q'_{0mb} (for bubbly water in the pipe) are greater than those between the real parts of k'_{1b} and q'_{0mb} across most of the frequency range. This is due to the fact that bubbles change the attenuation more effectively than they do the phase speed of media. Thus, in the present study, the extent of possible values of k'_{1b} was set to go from $0.5\mathrm{Re}[q'_{0mb}]$ to $2\mathrm{Re}[q'_{0mb}]$ in the real part, and from $0.1\mathrm{Im}[q'_{0mb}]$ to $1000\mathrm{Im}[q'_{0mb}]$ in the imaginary part, ranges which were estimated from the data in figure 1. Outside of these ranges, k'_{1b} was simply substituted with q'_{0mb}.

3. Experimental method

Experiments were carried out in a water-filled PMMA tube of 2 m length, 4.445 cm inner radius and 0.5 cm wall thickness which is supported vertically (Baik *et al.* 2010; Leighton *et al.* 2012). The driving frequency of the function generator, which does not necessarily equal the peak frequency of the energy in the water (Baik *et al.* 2010) was incremented from 15 to 35 kHz in 1 kHz steps, with 20 cycles per pulse. To obtain the sound speed and attenuation at each frequency, the two-dimensional Fourier Transform technique and Prony's method were adopted (Baik *et al.* 2010; Jiang *et al.* 2011).

Air was injected 15 cm above the tube base using a lumbar puncture needle (90 mm length and 0.6 mm outer diameter), the needle being vibrated using a mobile phone vibrator to prevent bubble coalescence at the needle tip (Leighton *et al.* 2011, 2012), changing the bubble radius range from 1–2.5 mm to approximately 30–1000 μm.

An optical method, called μCORT (Multi-Color Rise Time, a version of which also exists in monochrome—Leighton & White 2012) provided an independent (non-acoustical) estimate of the BSD by exposing each frame of the cloud of rising bubbles to a red flash, followed by a blue flash a short time later (0.025 s for figure 2; 0.042 s for the 0.0058% void fraction of figure 3). This removes the need to image the bubble wall accurately (and assume a given dimension in the third dimension) that are requirements of most photographic techniques for obtaining BSD, and therefore restricts them to the bubble size range that can be imaged accurately in the field of view. By eliminating that need, μCORT overcomes such limitations, expands the field of view and depth of field, and extends the bubble radius range. μCORT is immune to image distortion caused by the curvature of the pipe walls, and overcomes errors introduced by software that cannot recognize that what it might perceive to be a bubble perimeter in fact only extends to a highlight of the illumination on a fraction of the bubble wall. μCORT automatically calculates the rise speed of each of the thousands of bubbles in the field of view by correlating the locations of the neighbouring red and blue images in the frame to pair up automatically the images of the same bubble, and hence its displacement during the interval between the flashes. The potential errors come in then converting those rise speeds to bubble radii. While calibration curves exist which might allow conversion of rise speed into bubble size for air–water mixtures such as used here (Clift *et al.* 1978), the tendency of the bubbles to act collectively, and for the pipe geometry to affect rise speed (Krishna *et al.* 1999; Mukundakrishnan *et al.* 2007), must be considered. The rise times of bubbles in swarms in tubes of similar size to the one used here have been studied previously (Garnier *et al.* 2002; Simonnet *et al.* 2007). Given that Garnier *et al.* (2002), working with larger bubbles (up to 2.75 mm radius) at higher void fractions (1–40%) than used here (approx. 30–1000 μm and 0.005%, respectively) concluded that wall effects could be neglected in terms of rise speed, and that the results were applicable for void fractions of less than 1 per cent, that assumption is also applied here. However, Garnier *et al.* (2002) indicate that, for bubbles smaller than 2.75 mm radius, if an isolated bubble were to rise at a speed V_∞ in a quiescent liquid, then its equivalent rise speed (V_{rel}) relative to the liquid flow when it is part of a cloud of void fraction Γ is $V_{rel} = V_\infty(1 - \Gamma^{1/3})$. This correction was tested by Guet *et al.* (2004) for bubbles smaller than 3 mm
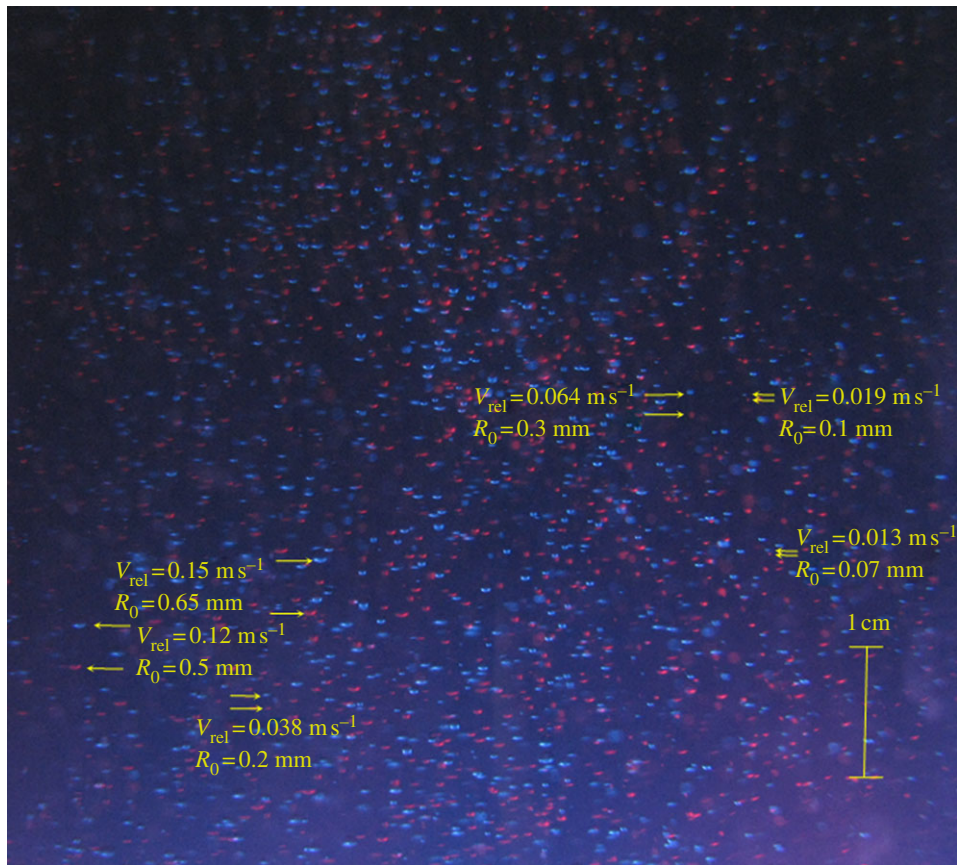
Figure 2. A single stills frame images each rising bubble twice by a red flash and then a blue flash 0.025 s afterwards, allowing calculation of the rise speed V_{rel} and hence the spherically equivalent bubble radius R_0. The void fraction calculated from this particular image was 3%.

radius and void fractions smaller than 20 per cent (scenarios which cover the current case). This correction, though small (approx. 4%) for the void fractions (less than 10^{-4}) studied here, is applied in this paper.

The effect of containment in a pipe on bubble resonance is rarely calculated (Leighton *et al.* 1998*a*, 2002). Using the worst case formulations of Leighton (2011), neglect of this effect causes a systematic error which underestimates the bubble inertia associated with its pulsation resonance by 3 per cent for bubble radii of 30 µm, rising to approximately 100 per cent for bubble of radius 1mm. However, the lowest frequency applied to the population is here 15 kHz, corresponding to a resonance with a bubble of radius approximately 200 µm where the inertia is underestimated by 20 per cent. Though significant, an iteration step was not applied to undertake this correction because it was small compared with the error discussed in §4.

The grey solid curve in figure 3 shows the raw optical BSD (bubble population present during the acoustic tests) obtained by the µCORT method. In order to obtain smooth curves of calculations for bubbly media, raw optical BSD
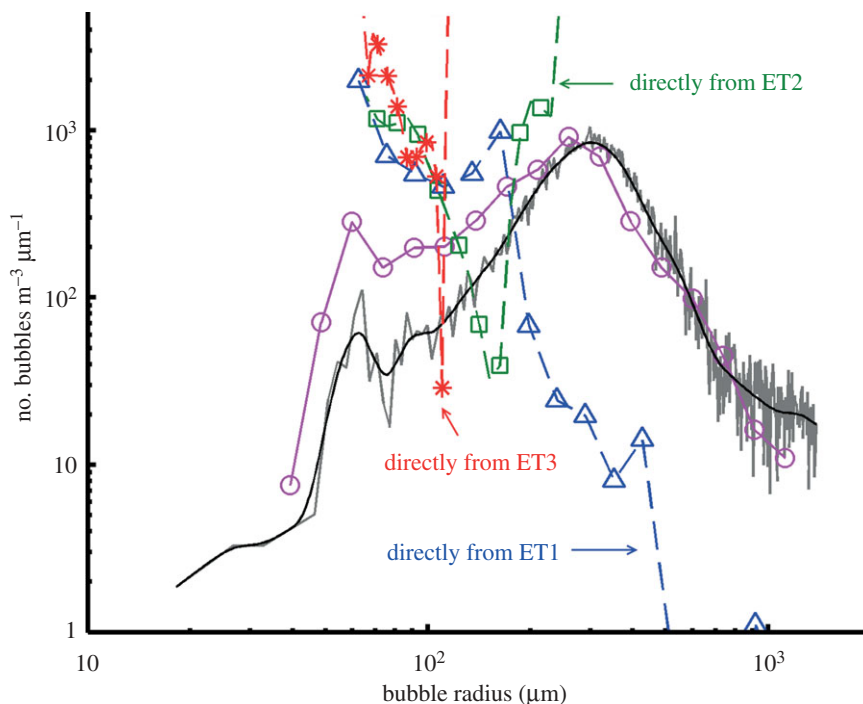
Figure 3. The bubble size distribution (BSD) measured by the μCORT method is shown by a solid grey line. After filtering, it becomes smoother (solid black line) and this was used as a reference BSD in this study. A 10 megapixel camera with the field of view used here could measure the rise speed of bubbles as small as $10\,\mu$m although, rather than a strict cut-off, undercounting will become progressively worse as this limit is reached. These data are then used to predict sound speeds and attenuations for figure 1, then inverted *in the standard manner* (i.e. *under the assumption that the data were taken under PWFF conditions*) to recover an estimate of the BSD. Open circles are used to plot the BSD estimated by an acoustic inversion using the theoretical complex wavenumber for the free field bulk bubbly water (the dashed curves in figure 1c,d), free field being assumed both for the forward problem (to generate the dashed curves in figure 1c,d) and the inverse problem, to generate the open-circle curve here. Agreement is good because the assumptions of the inversion match those of the inversion. However, for the other curves on this plot (ET1 (triangles), ET2 (squares) and ET3 (asterisks)) the free field assumption of the inversion do not match the in-pipe conditions used to generate the data for these modes in figure 1. This corresponds to applying the standard free field inversion to data taken in pipes. (Online version in colour.)

is digital filtered to produce the black solid curve, which is the BSD adopted throughout this paper. The meanings of other symbols (circles, triangles, squares and asterisks) are explained in the figure caption and §4a. Note that the average bubble radius is approximately $300\,\mu$m, and for such bubbles the resonance frequency (approx. $10\,$kHz) is lower than the lowest frequency the affordable acoustical source can generate, illustrating the practical limitations of acoustic inversions of this type. This BSD has a gas volume void fraction of $\Gamma \approx 0.0058\%$.

4. Results

(a) Validation tests using simulated acoustic data based on optical measurements

The optical (μCORT) estimation of the BSD that occurred in the pipe during the acoustical tests (the black solid line in figure 3) was used as input in the forward model of Commander & Prosperetti (1989) (equation (2.1) in this paper) to predict what phase speed and extra attenuation the bubbles would have generated for PWFF propagation in an infinite body of water (the dashed curves in figure 1c,d). When these dashed line data in figure 1c,d are used as input in an inversion which assumes an infinite body of bubbly liquid following the method of Commander & McDonald (1991), equation (2.3), that inversion of course recovers the BSD used as the original input (the open circles in figure 3, with characteristic discrepancies at the ends of the size range illustrating the error introduced by the inversion itself). Such agreement is of course meaningless to the circumstances that actually exist in the pipe.

However, the importance of figure 3, and the *raison d'être* of this paper, is in showing what would happen if sound speed and attenuation data taken in a pipe were to be used to estimate the BSD under the traditional assumption of PWFF conditions. The acoustic data are simulated (the ET1, ET2 and ET3 solid curves in figure 1, calculated using the theory of Baik *et al.* 2010) because that allows us to know the actual BSD data used as input (solid black line in figure 3), against which we can compare the BSD estimated using PWFF theory in the traditional manner. The inversion proceeds as follows. The predicted complex wavenumber of the ET1, ET2 and ET3 modes for bubbly conditions (the solid curves in figure 1) are directly used as simulated input data Y_ψ. These data are then inverted using equation (2.3) for the inversion (which assumes an infinite body of liquid). Since the in-pipe conditions under which the solid line ET1, ET2 and ET3 acoustic data of figure 1 where 'measured' are not matched by the PWFF assumptions of equation (2.3), the estimates of the BSD are expected to be wildly erroneous. This is indeed shown to be the case in figure 3 for ET1 (triangles), ET2 (squares) and ET3 (asterisks). This demonstrates that the traditional inversion technique, uncorrected for deviations from PWFF conditions, cannot be assumed to be accurate when such deviations occur. For example, the ET1 data (triangles) above approximately 200 μm radius in figure 3 record more than 1000 per cent undercounts, while the other symbols (squares and asterisks) record more than 1000 per cent overcounts (too large to be plotted within the window of the figure). Therefore, the standard PWFF inversion can produce large errors in the estimation of the actual BSD inside the pipeline.

There is, however, a solution. As explained by equation (2.9), the complex wavenumbers that would have occurred were the same BSD present in PWFF conditions can be inferred from figure 1's simulated data for the phase speed and the attenuation of the modes in a pipe containing that same BSD. This can be used to ensure that the inversion is undertaken on data which complies with the assumptions inherent in that inversion. Since PWFF conditions never exist in practice in bubbly liquids, strictly speaking no such inversion for BSD from travelling wave attenuations and sound speed has ever done this, although clearly under some circumstances the approximation is sufficiently good (Wilson *et al.* 2005). Note however that the method here does not account for the effects on

the bubble dynamics themselves of the wall of a tank (Strasberg 1953; Leighton *et al.* 2002) or pipe (Leighton *et al.* 1995, 1997, 1998*b*, 2000; Leighton 2011), or the departure from linearity or steady-state conditions (Clarke & Leighton 2000), all of which could be included given sufficient computational resources (Leighton *et al.* 2004). Figure 4*a* plots Y_ψ, the ratio of the imaginary part to the real part of the complex wavenumber as defined in equation (2.4), for infinite volumes of homogeneous bubbly liquid. The dashed line is the value of Y_ψ that would have been obtained if the BSD that occurred in the pipe (figure 3, black solid line) were to have existed in just such an infinite body of liquid. The open symbols and asterisks are the result of using equation (2.9) to convert the measured Y_ψ of the various modes in the pipe into approximate values appropriate for an infinite volume of bubbly liquid. The shape of the ET1 result (triangles) is similar to the dashed curve except an abrupt peak around $k_1 a \approx 3.4$, where the break point (the frequency where the phase speeds of the ET1 and ET2 modes (the solid lines in figure 1*a*) approach closest with each other, Baik *et al.* 2010) is observed. In the frequency range of $k_1 a < 2$, the approximated Y_ψ is greater than the dashed curve by the factor of about 10 (experienced users will often discard end-of-range data because such effects are expected). Except for these two frequency ranges, the approximated Y_ψ converted from the ET1 mode is similar to the attenuation in PWFF bubbly liquid. Since equation (2.9) assumes small deviations between axial wavenumbers, q'_{0mf} and q'_{0mb}, and between free field wavenumbers, k'_{1f} and k'_{1b}, wherever these conditions are disobeyed, the approximation inherent in equation (2.9) does not work well. Therefore, conversion from the ET1 mode gives a large discrepancy near $k_1 a \approx 3.4$ where the difference between q'_{0mf} and q'_{0mb} becomes greatest. This can be seen from figure 1, recalling that the normalized phase speed C_{0m}/C_1 is calculated from $k_1/\mathrm{Re}[q'_{0m}]$, where Re represents real part and q'_{0m} is either q'_{0mf} or q'_{0mb}. In figure 1, $k_1 a \approx 3.4$ represents the location where the separation between the ET1 solid and dashed sound speed curves in (*a*) becomes greatest, and where attenuation in (*b*) peaks. A similar large discrepancy between these two curves is also observed in figure 1*a* for $k_1 a < 2$ where the difference between k'_{1f} and k'_{1b} is large for the ET1 mode. Use of the Y_ψ data from the other modes (ET2 (squares) and ET3 (asterisks)) produces poorer agreement. The ratio Y_ψ converted from the ET2 mode (squares) is far from the free field Y_ψ for an infinite bubbly liquid (dashed curve) and, moreover, it gives negative values for Y_ψ around $k_1 a \sim 4.4$ (which are not displayed in this picture). The same trend is investigated in the ET3 result around $k_1 a \sim 8$. This level of agreement illustrates the difficulties inherent in comparing the values of Y_ψ measured in real scenarios with those predicted by PWFF theory.

The converted Y_ψ plot is then used in the acoustic inversion using linear matrix representation in equation (2.3). The input ratio, Y_ψ, represents the bubble-induced change of complex wavenumber between in bulk bubbly liquid and in bulk bubble-free liquid (both being in PWFF conditions). For laboratory experiments using the frequency span and source-to-receiver separations used here, the attenuation in an infinite body of bubble-free liquid is usually negligible (at least 1000 times smaller than that in bubbly water), which means Y_ψ is very small. Since use of equation (2.9) shows greatest success in converting the Y_ψ of the ET1 mode, it is not surprising that when this converted Y_ψ (triangles) is used in the inversion (that assumes an infinite body of homogeneous bubbly liquid) in figure 4*b*, it is most successful at predicting the actual BSD that was
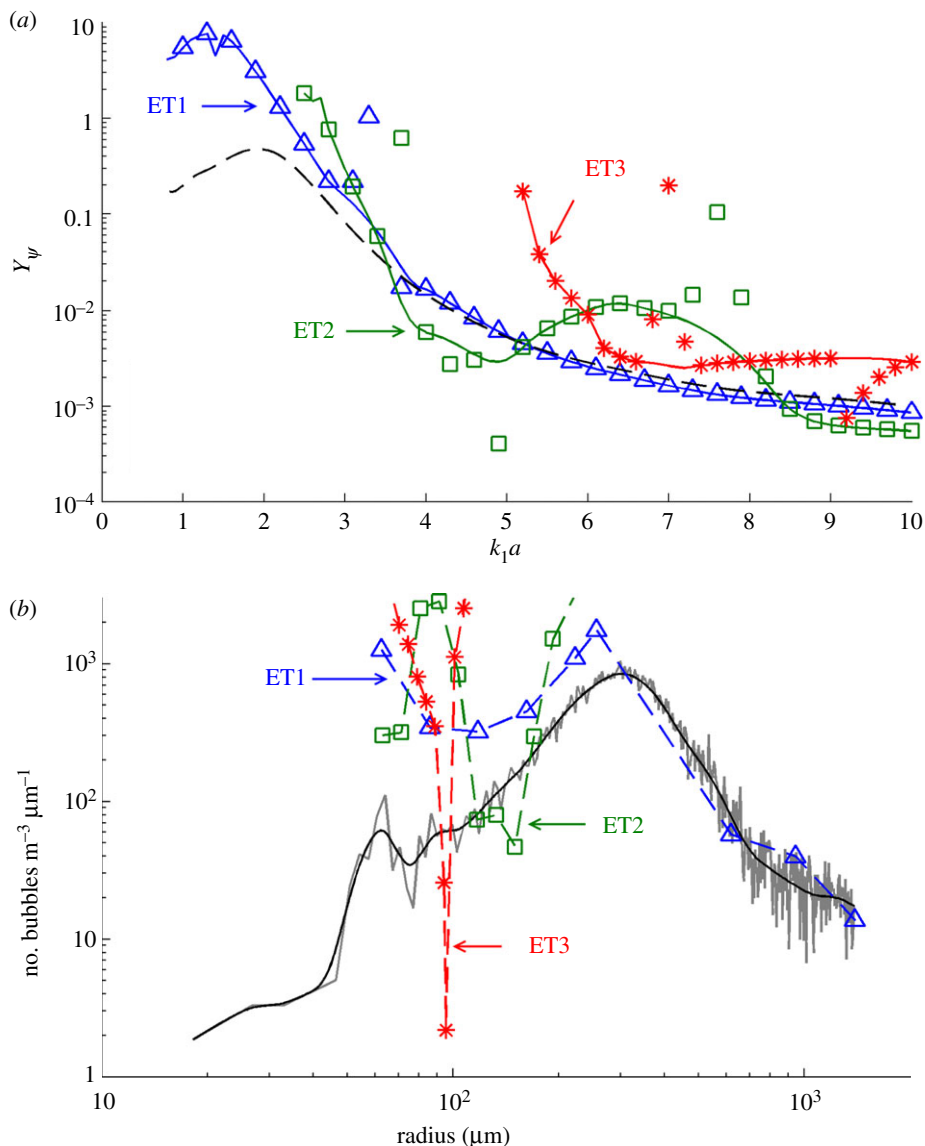
Figure 4. (*a*) The ratio Y_ψ defined just after eqn (2.4) in bulk bubbly liquid (dashed curve) and the approximation to Y_ψ obtained by using eqn (2.9) to convert the data in figure 1 from the ET1 (triangles), ET2 (squares) and ET3 (asterisks) modes (i.e. using eqn (2.9) to estimate the complex wavenumbers in bubble-free liquid, and then calculating Y_ψ from the ratio of the imaginary to the real part of such estimated complex wavenumbers). All solid curves are obtained by removing sudden peaks or dips observed in the raw converted data (as shown in the open symbols and asterisks) and filling removed data by the interpolation. (*b*) The actual bubble size spectrum (the solid black curve) and the BSD obtained by the acoustic inversion when the converted complex wavenumbers from the ET1, ET2 and ET3 modes seen above are used. (Online version in colour.)

measured optically. Indeed, the level of agreement is similar to that shown here for the standard technique, when data from actual PWFF conditions (the dashed curves in figure 1*c,d*) is inverted using the PWFF inversion to generate the BSD

shown by the open circles in figure 3. The other modes (squares for ET2, asterisks for ET3) are, unsurprisingly, less successful in their estimates in figure 4b of the BSD, because their estimates of Y_ψ were less good in figure 4a.

It is sensible in such inversions to eliminate unphysical peaks (such as that seen in the ET1 mode (triangles) around $k_1 a \approx 3.4$), typical of inversion artefacts, and fill the resulting absent region with the interpolated Y_ψ using the remaining smooth raw data (greater regularization would eliminate such artefacts but smooths data unnecessarily, so good practice is to add just enough regularization to make the last negative bubble count turn positive, then eliminate likely artefact peaks).

Using identical symbols schemes, figures 3 and 4b, respectively, show the BSDs obtained from the processed (by equation (2.9)) and the unprocessed modes. Of the three modes tested, the ET1 mode (triangles) produces an estimate from this new approach (triangles in figure 4b) that is closer to the actual BSD than simply using the unprocessed ET1 attenuation (triangles in figure 3). While the BSDs obtained from the processed ET2 and the ET3 modes still give poor results, as expected, they illustrate the cause of this error: the fact that in order to obtain a good estimate of BSD, the lowest frequency for which data is available must be lower than the pulsation resonance of the largest bubble present in the population, as discussed earlier. The cut-off frequencies of the ET2 and the ET3 modes are around $k_1 a = 3$ and $k_1 a = 5.5$, respectively, corresponding to resonance frequencies of 200 and 100 µm radius bubbles. Because there is therefore no information for Y_ψ at lower frequencies than these cut-offs for each mode, the acoustic inversion of the modes only gives finite bubble counts in figure 4b for bubbles smaller than the radii corresponding to these cut-off frequencies. Although it is possible to obtain estimates of the BSD above these radii, those are expected to be highly ill-posed despite regularization. Therefore, in order to get the best estimation of the BSD, it is necessary to have a measurement of the Y_ψ at frequencies less than the resonance frequency of the largest radius of the bubble in the BSD. This is a challenging requirement experimentally, since for a given broadband source, the cost per octave is roughly constant with today's manufacturers, making the low-frequency region particularly problematic: it costs roughly as much to cover the 1.5–3 kHz band as it does to cover the 20–40 kHz band. To save cost, experimenters will choose a low-frequency limit for their sources, but should not then apply this system unless they know that no bubbles with resonances lower than this low-frequency limit will be present. Use of optical techniques to measure the larger bubble sizes, can mitigate this problem. Optical techniques can fail to resolve the smallest bubbles but become more accurate and cost-effective for larger ones. In this way, they exhibit the opposite trend to acoustic methods, and are therefore complementary to acoustic techniques. The proposition that parametric sonar might be applied to explore the low-frequency regime is complicated by the fact that bubbles affect the parametric sonar operation itself, not just the wave once generated.

(*b*) *Acoustic measurements*

Section 4a illustrated how difficult is the problem of inferring BSDs using acoustic inversion in a pipe when the data are simulated (and so covers the full frequency range without gaps). Real measurements produce less idealized

coverage, and hence the problems of using it in an inversion are greater. The original design for this system commissioned transducers (that would wet when immersed in mercury, but not react with it) covering the 1 kHz–1 MHz frequency range, but this was no longer affordable after the 2008 global financial crash. Therefore, the current exercise was conducted to see if the affordable bandwidth was worth purchasing. Figure 5 shows the measurements of phase speed and the attenuation of the ET1 (triangles), ET2 (squares) and ET3 (asterisks) modes taken in the bubbly water-filled PMMA pipe. The theoretical dispersion curves under the BSD in figure 3 (black solid curve) are calculated from the theory of Baik *et al.* (2010) and plotted for comparison as solid curves. Although all three modes produce theoretical curves across the frequency range studied, in practice certain modes are observed preferentially in particular frequency ranges for the reasons discussed by Baik *et al.* (2010). It should be noted that although the pipe used here is the same as that used in Baik *et al.* (2010), the frequency ranges over which modes are observed change because figure 5 is for bubbly water whereas Baik *et al.* (2010) made measurements in bubble-free water. The ET1 mode is only observed above the frequency of $k_1 a \sim 3.5$. Below that frequency, the ET2 mode is observed instead. The ET2 mode is again observed above $k_1 a \sim 6.5$. The ET3 mode is observed below this frequency and its phase speed becomes infinite when the acoustic excitation is close to the cut-off frequency of the ET3 mode. Compared with the agreement seen in the ET2 and ET3 measurements, the phase speed of the ET1 modes in figure 5*a* was measured to be generally less than the theoretical prediction.

Figure 5*b* shows the measurement of the attenuation of the modes, using the same symbol notation as for figure 5*a*. As discussed by Baik *et al.* (2010), the attenuation obtained from Prony's method is sensitive to the sampling range along the axis of the tube (where the z_1 and z_2 locations of hydrophone along the tube axis represent the start and endpoints of the sampling). The error bars represent ± 1s.d. in the mean of results obtained by taking different sampling ranges for $|z_2 - z_1|$ from 0.3 to 1.3 m in 1 cm increments. Although error bars are also plotted in figure 5*a*, those are very small and mostly extend inside the markers (Baik *et al.* 2010). Although at first sight, the experimental data appear to follow the theoretical predictions, validating the theory, the degree of validation must be tempered by the large size of the error bars, as was predicted by Baik *et al.* (2010). In reality, the large error bars imply that all that can conclusively be stated is that the data do not contradict the theory proposed in this study.

Since $Y_\psi = v_\psi / u_\psi$ is the quantity which is used in the inversion, attenuation associated with v_ψ must be neither so great that there is poor SNR, nor so small that the value of the Y_ψ parameter fed into the inversion has a proportionally massive uncertainty. Because of this, and because it does not have a cut-off frequency (and therefore incorporates information about the large bubbles), the ET1 mode is the most useful of those measured here for inferring the BSD. In fact, a peculiarity of the actual measurement conducted here relates to the issue mentioned above, whereby unlike the simulated data tests of the previous section, the real dataset is incomplete. The peculiar consequence here is that, in the frequency range over which signal for ET1 is detectable ($3.9 < k_1 a < 6.2$), its attenuation is almost identical to that which the optically measured BSD would give in an infinite body of bubbly water (figure 1). Therefore, one would not expect this ET1 data to be affected much by conversion through equation (2.9),
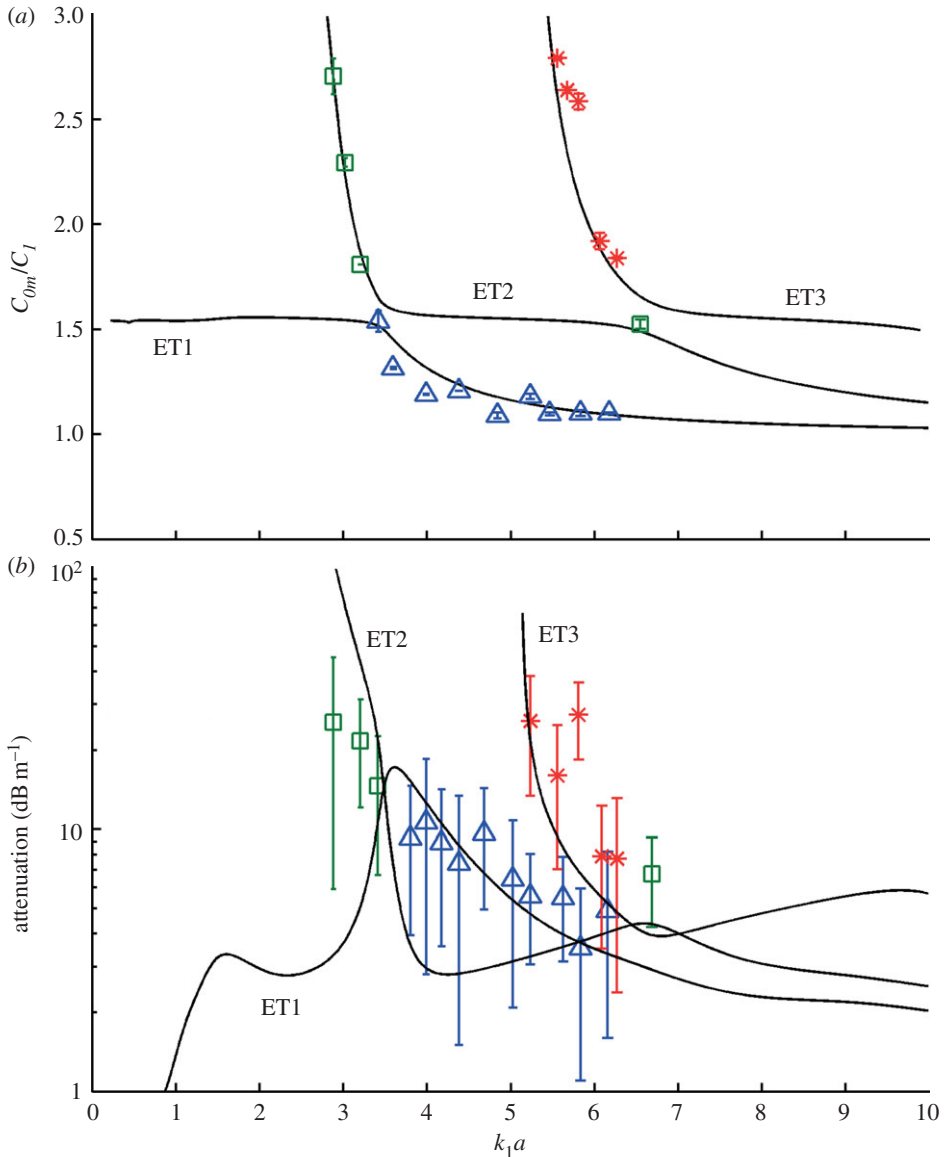
Figure 5. Phase speeds in (*a*) and the attenuations in (*b*) of the modes. Solid curves are theoretical predictions of the axisymmetric modes in the PMMA tube filled with the bubbly water which has a BSD given by the black solid curve in figure 3. Measurements (in the PMMA pipe filled with bubbly water) are for the ET1 (triangles), ET2 (squares) and ET3 (asterisks) modes. Error bars represent ± 1 s.d. in the mean (each point being an average of 101 measurements). The error bars in sound speed in (*a*) are no larger than the size of the symbol. (Online version in colour.)

and then to give a reasonable estimate of BSD over a limited range of bubble sizes. Figure 6*a* shows the converted Y_ψ from the average of measured Y_ψ (ET1 (triangles), ET2 (squares) and ET3 (asterisks)) by the process in equation (2.9). The theoretical Y_ψ in the infinite body of bubbly water with the measured BSD
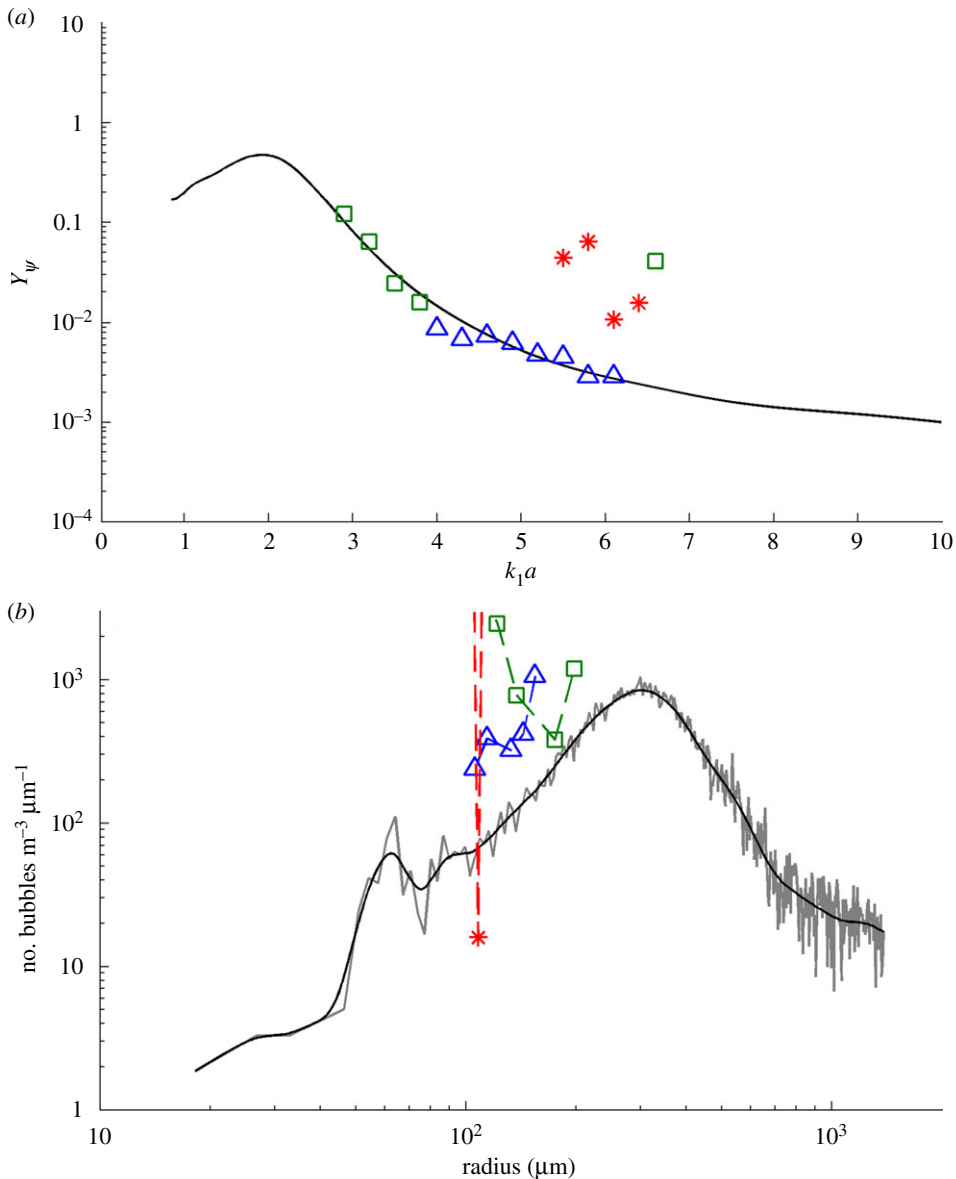
Figure 6. (*a*) Estimations of the Y_ψ that would have occurred in free field bulk bubbly water by eqn (2.9), obtained by converting the measured Y_ψ data of the ET1 (triangles), ET2 (squares) and ET3 (asterisks) modes. The theoretical Y_ψ in bulk bubbly water with the measured optical BSD (black solid curve in (*b*)) is superposed as a solid curve. (*b*) The optically measured BSD (black solid curve; the grey solid line shows measured raw data) and the acoustic BSDs (open symbols and asterisks connected by dashed lines) obtained from each measured Y_ψ of (*a*). (Online version in colour.)

inside the pipe (black solid curve in figure 6*b*) is represented by solid curve. When these data in figure 6*a* are used in the acoustic inversion, the result is displayed using the same symbols in figure 6*b*. Since the measurement of the ET1 mode

is only obtained in the frequency range of $3.9 < k_1 a < 6.2$ (equivalent to 20.6 to 32.8 kHz), the corresponding BSD estimation spans only from approximately 100 to 150 μm radius, which are bubble sizes giving those resonance frequencies. Therefore, the BSD obtained from our measurement is limited to this bubble size range. For such small size ranges, the end-of-range errors that are known to occur with such inversions (and cause divergence of the result at the end of the range) are given undue prominence: as expected therefore, closest agreement between the optically measure BSD and that obtained from the acoustic inversion occurs in the middle of the acoustic range. In order to obtain the BSD of the other radii of the bubbles, it is necessary to measure the Y_ψ over a wider bandwidth. The estimated BSD obtained from the measurement of the bubbly cylinder is greater than the actual BSD by the factor of from 2 to 4. In this frequency range, the same trend is observed in figure 4b when the theoretical ET1 Y_ψ in bubbly cylinder was directly used in the acoustic inversion. However, as mentioned above, the theoretical ET1 Y_ψ in this frequency range is not far from the free field Y_ψ in bulk bubbly water. When the theoretical free field Y_ψ was used in the acoustic inversion instead, the estimated BSD is close to the actual BSD as shown by the open circles in figure 3. Therefore, the BSD in this corresponding radius range (from approx. 100 to 150 μm) is very sensitive to the Y_ψ in the corresponding frequency range (from 20.6 to 32.8 kHz). Consequently, a more precise measurement is required to estimate the correct BSD by the acoustic inversion. However, more precise measurements in this bubble radius range (or corresponding frequency range) do not significantly change the gas volume void fraction since the greatest contribution to the void fraction comes from the larger bubbles, the resonance frequencies of which are far below this frequency range.

The BSDs estimated from the higher modes ET2 (squares) and ET3 (asterisks) are also plotted in figure 6b. One might expect a poor estimate of the BSD from ET3, because the converted values of Y_ψ for this mode (the asterisks in figure 6a) are far from the theoretical free field Y_ψ in bulk bubbly water. Although part of the measurement of ET3 is obtained beyond the frequency range of the measured ET1 mode ($k_1 a \sim 6.4$), and so might have been potentially useful in extending the range of bubble sizes estimated, the accuracy of those estimations (the asterisks in figure 6b) do not agree well with the actual BSD. (Indeed, although the BSD estimated from the ET3 mode spans to a higher frequency range than that covered by the ET1 mode, the BSD data points corresponding to these smaller bubbles sizes are not plotted in this figure because (at $n_b(R_0) \sim 10^4 \, \mathrm{m}^{-3} \, \mu\mathrm{m}^{-1}$) the values are out of range of the plotted bubble concentrations). The same trend is observed for ET2 mode when the data at $k_1 a \sim 6.6$ were used for the acoustic inversion (the corresponding frequency resonates with bubbles of approx. 90 μm radius), which gives BSD estimations (squares) that do not agree with the solid BSD curve. However, the converted values of Y_ψ from the measurement of the ET2 mode (squares in figure 6a) are very close to the theoretical free field Y_ψ for a bulk bubbly liquid in the range of $2.9 < k_1 a < 3.9$ which corresponds to frequencies that are resonant with bubbles having radii from approximately 150 to 210 μm. Consequently, the BSD estimated from the ET2 mode in the bubble radius range of approximately 150–210 μm (the two squares in figure 6b) are close to the black solid BSD curve. As expected, there is much poorer agreement for the estimations of BSD from bubbles that are smaller than approximately 150 μm radius for the ET2 mode. Because of the missing data in the range of $3.9 < k_1 a < 6.5$, these

estimates were obtained from the interpolation using existing ET2 data, which is, of course, far from the theoretical Y_ψ, and therefore gives poor agreement with the actual BSD over the corresponding bubble size range (radii from approx. 90 to 150 µm).

5. Conclusions

Simulated and real data were used to explore how measured phase speeds and attenuations in bubbly liquid in a pipe might be inverted to estimate the BSD (which was independently measured using an optical technique). Use of the standard PWFF theory generated large errors when applied to data in pipes. A new inversion used a Taylor series to relate the complex wavenumber measured in a pipe to what would, for the same BSD, have been measured in an infinite homogenous volume of bubbly liquid. When simulated data for the frequency range originally planned for the sensor were used, the new inversion performed well. However, it performed poorly when using actual data from the more narrow frequency range that could be afforded, the result being dominated by the known end-of-range errors that occur during such inversions. The conclusion is that it is not worth ORNL commissioning a sensor with this reduced frequency range, because although it is affordable, the loss of accuracy is unacceptable While such errors can be identified by using complementary optical techniques, this is not possible in optically opaque media and pipelines (although the authors developed an optical fibre which detected bubbles in mercury, a system which provided statistically significant sampling was unaffordable). It is therefore important to question the accuracy of estimated BSDs particularly when they inform high-value decisions by industry. The planned addition of a controlled population of helium bubbles to ORNL's SNS TTF in 2013 is designed to mitigate damage to the target, and so prolong the period between which the target is replaced. The cost of a failed target could amount to £12 M, including $800 k for the new target, $200 k for disposal of the old (now radioactive) target, and the cost of interruption to the use of the facility (B. Riemer 2012, personal communication). The method in this paper allowed industry to assess beforehand the cost/benefit of employing a given inversion technique, including the cost of insufficient investment in a wide enough frequency range.

References

Ainslie, M. A. & Leighton, T. G. 2011 Review of theory for scattering and extinction cross-sections, damping factors and resonance frequencies of spherical gas bubbles. *J. Acoust. Soc. Am.* **130**, 3184–3208. (doi:10.1121/1.3628321)

Baik, K., Jiang, J. & Leighton, T. G. 2009 Theoretical investigation of phase velocity, group velocity and attenuation of acoustic waves in a liquid-filled cylinder, 40 pp. ISVR Technical Report 329, University of Southampton, Southampton, UK.

Baik, K., Jiang, J. & Leighton, T. G. 2010 Acoustic attenuation, phase and group velocities in liquid-filled pipes: theory, experiment, and examples of water and mercury. *J. Acoust. Soc. Am.* **128**, 2610–2624. (doi:10.1121/1.3495943)

Campbell, G. M. & Mougeot, E. 1999 Creation and characterisation of aerated food products. *Trends Food Sci. Technol.* **10**, 283–296. (doi:10.1016/S0924-2244(00)00008-X)

Caruthers, J. W., Elmore, P. A., Novarini, J. C. & Goodman, R. R. 1999 An iterative approach for approximating bubble distributions from attenuation measurements. *J. Acoust. Soc. Am.* **106**, 185–189. (doi:10.1121/1.427047)

Chitnis, P. V., Manzi, N. J., Cleveland, R. O., Roy, R. A. & Holt, R. G. 2010 Mitigation of damage to solid surfaces from the collapse of cavitation bubble clouds. *J. Fluids Eng.* **132**, 051303. (doi:10.1115/1.4001552)

Clarke, J. W. L. & Leighton, T. G. 2000 A method for estimating time-dependent acoustic cross-sections of bubbles and bubble clouds prior to the steady state. *J. Acoust. Soc. Am.* **107**, 1922–1929. (doi:10.1121/1.428474)

Clift, R. Grace, J. R. & Weber, M. E. 1978 *Bubbles, drops, and particles*. New York, NY: Academic Press.

Commander, K. W. & McDonald, R. J. 1991 Finite-element solution of the inverse problem in bubble swarm acoustics. *J. Acoust. Soc. Am.* **89**, 592–597. (doi:10.1121/1.400671)

Commander, K. W. & Prosperetti, A. 1989 Linear pressure waves in bubbly liquids: comparison between theory and experiments. *J. Acoust. Soc. Am.* **85**, 732–746. (doi:10.1121/1.397599)

Duraiswami, R., Prabhukumar, S. & Chahine, G. L. 1998 Bubble counting using an inverse acoustic scattering method. *J. Acoust. Soc. Am.* **104**, 2699–2717. (doi:10.1121/1.423854)

Farmer, D. M., Vagle, S. & Booth, D. 2005 Reverberation effects in acoustical resonators used for bubble measurements. *J. Acoust. Soc. Am.* **118**, 2954–2960. (doi:10.1121/1.2047148)

Garnier, C., Lance, M. & Marie, J. 2002 CFD simulation of sparger design and height to diameter ratio on gas hold-up profiles in bubble column reactors. *Exp. Thermal Fluid Sci.* **28**, 407–421.

Guet, S., Ooms, G., Oliemans, R. V. A. & Mudde, R. F. 2004 Bubble size effect on low liquid input drift-flux parameters. *Chem. Eng. Sci.* **59**, 3315–3329. (doi:10.1016/j.ces.2004.03.036)

Hansen, P. C. 1998 *Rank-deficient and discrete ill-posed problems: numerical aspects of linear inversion.* Philadelphia, PA: SIAM.

Hansen, G., Butzek, M., Glückler, H., Hanslik, R., Soltner, H., Soukhanov, V., Stelzer, H. & Wolters, J. 2004 Engineering Work for the ESS Target Station. In *Proc. 6th Int. Topical Meeting on Nuclear Applications of Accelerator Technology 'Accelerator Applications in a Nuclear Renaissance', San Diego, CA, USA, AccApp'03, 1–5 June, 2003*, pp. 452–463. La Grange Park, IL: American Nuclear Society.

Iskandrani, A., & Kojasoy, G. 2001 Local void fraction and velocity field description in horizontal bubbly flow. *Nuclear Eng. Design* **204**, 117–128. (doi:10.1016/S0029-5493(00)00361-7)

Jiang, J., Baik, K. & Leighton, T. G. 2011 Acoustic attenuation, phase and group velocities in liquid-filled pipes II. Simulation for spallation neutron sources and planetary exploration. *J. Acoust. Soc. Am.* **130**, 695–706. (doi:10.1121/1.3598463)

Kargl, S. G. 2002 Effective medium approach to linear acoustics in bubbly liquids. *J. Acoust. Soc. Am.* **111**, 168–173. (doi:10.1121/1.1427356)

Krishna, R., Urseanu, M. I. van Baten, J. M. & Ellenberger, J. 1999 Wall effects on the rise of single gas bubbles in liquids. *Int. Comm. Heat Mass Transfer* **26**, 781–790. (doi:10.1016/S0735-1933(99)00066-4)

Lafleur, L. D. & Shields, F. D. 1995 Low-frequency propagation modes in a liquid-filled elastic tube waveguide. *J. Acoust. Soc. Am.* **97**, 1435–1445. (doi:10.1121/1.412981)

Leighton, T. G. 2011 The inertial terms in equations of motion for bubbles in tubular vessels or between plates. *J. Acoust. Soc. Am.* **130**, 3333–3338. (doi:10.1121/1.3638132)

Leighton, T. G. & Robb, G. B. N. 2008 Preliminary mapping of void fractions and sound speeds in gassy marine sediments from subbottom profiles. *J. Acoust. Soc. Am.* **124**, EL313–EL320. (doi:10.1121/1.2993744)

Leighton, T. G. & White, P. R. 2012 Quantification of undersea gas leaks from carbon capture and storage facilities, from pipelines and from methane seeps, by their acoustic emissions. *Proc. R. Soc. A* **468**, 485–510. (doi:10.1098/rspa.2011.0221)

Leighton, T. G., White, P. R. & Marsden, M. A. 1995 Applications of one-dimensional bubbles to lithotripsy, and to diver response to low frequency sound. *Acta Acust.* **3**, 517–529.

Leighton, T. G., Ho, W. L. & Flaxman, R. 1997 Sonoluminescence from the unstable collapse of a conical bubble. *Ultrasonics* **35**, 399–405. (doi:10.1016/S0041-624X(97)00014-0)

Leighton, T. G., Ramble, D. G., Phelps, A. D., Morfey, C. L. & Harris, P. P. 1998*a* Acoustic detection of gas bubbles in a pipe. *Acustica* **84**, 801–814.

Leighton, T. G., Phelps, A. D., Cox, B. T. & Ho, W. L. 1998*b* Theory and preliminary measurements of the Rayleigh-like collapse of a conical bubble. *Acustica* **84**, 1014–1024.

Leighton, T. G., Cox, B. T. & Phelps, A. D. 2000 The Rayleigh-like collapse of a conical bubble. *J. Acoust. Soc. Am.* **107**, 130–142. (doi:10.1121/1.428296)

Leighton, T. G., White, P. R., Morfey, C. L., Clarke, J. W. L., Heald, G. J., Dumbrell, H. A. & Holland, K. R. 2002 The effect of reverberation on the damping of bubbles. *J. Acoust. Soc. Am.* **112**, 1366–1376. (doi:10.1121/1.1501895)

Leighton, T. G., Meers, S. D. & White, P. R. 2004 Propagation through nonlinear time dependent bubble clouds, and the estimation of bubble populations from measured acoustic characteristics. *Proc. R. Soc. A* **460**, 2521–2550. (doi:10.1098/rspa.2004.1298)

Leighton, T. G., Jiang, J. & Baik, K. 2011 A TV demonstration of sound absorption connecting the space shuttle to submarines. *Acoust. Bull.* **36**, 35–40.

Leighton, T. G., Jiang, J. & Baik, K. 2012 Demonstration comparing sound wave attenuation inside pipes containing bubbly water and water droplet fog. *J. Acoust. Soc. Am.* **131**, 2413–2421. (doi:10.1121/1.3676732).

Mallock, A. 1910 The damping of sound by frothy liquids. *Proc. R. Soc. Lond. A* **84**, 391–395. (doi:10.1098/rspa.1910.0085)

Manzi, N. J., Chitnis, P. V., Holt, R. G., Roy, R. A., Cleveland, R. O., Riemer, B. & Wendel, M. 2010 Detecting cavitation in mercury exposed to a high-energy pulsed proton beam. *J. Acoust. Soc. Am.* **127**, 2231–2239. (doi:10.1121/1.3353095)

Mukundakrishnan, K., Ayyaswamy, P. S., Quan, S. & Eckmann, D. M. 2007 Numerical study of wall effects on buoyant gas-bubble rise in a liquid-filled finite cylinder. *Phys. Rev. Lett. E* **76**, 036308. (doi:10.1103/PhysRevE.76.036308)

Ormonde, C., Chitnis, P., Cleveland, R. O., Holt, R. G. & Roy, R. A. 2008 *A vertical acoustic waveguide for two-phase mercury-helium flow void fraction determination.* IMECE2008, abstract No. 66791, p. 196. New York, NY: American Society of Mechanical Engineers.

Punurai, W., Jarzynski, J., Qu, J., Kurtis, K. E. & Jacobs, L. J. 2006 Characterization of entrained air voids in cement paste with scattered ultrasound. *NDT E Int.* **39**, 514–524. (doi:10.1016/j.ndteint.2006.02.001)

Rath, H. J. 1981 Unsteady pressure waves and shock waves in elastic tubes containing bubbly air-water mixtures. *Acta Mech.* **38**, 1–17. (doi:10.1007/BF01351459)

Roy, R. A., Ormonde, C. E., Chitnis, P. V., Cleveland, R. O. & Holt, R. G. 2008 An acoustic resonator for determining the void fraction of bubbly mercury flows. *J. Acoust. Soc. Am.* **123**, 3559 (abstract). (doi:10.1121/1.2934597)

Schubert, B. S. V. 1991 Sound waves in an elastic tube containing a gas-droplet or a liquid-bubble mixture. *Acta Mech.* **87**, 81–92. (doi:10.1007/BF01177174)

Simonnet, M., Gentric, C., Olmos, E. & Midoux, N. 2007 Experimental determination of the drag coefficient in a swarm of bubbles. *Chem. Eng. Sci.* **64**, 858–866. (doi:10.1016/j.ces.2006.10.012)

Strasberg, M. 1953 The pulsation frequency of nonspherical gas bubbles in liquids. *J. Acoust. Soc. Am.* **25**, 536–537. (doi:10.1121/1.1907076)

Tikhonov, A. N. & Arsenin, V. Y. 1977 *Solution of ill-posed problems.* New York, NY: Wiley.

Vagle, S. & Farmer, D. M. 1998 A comparison of four methods for bubble size and void fraction measurements. *IEEE J. Oceanic Eng.* **23**, 211–222. (doi:10.1109/48.701193)

Wilson, P. S. Roy, R. A. & Carey, W. M. 2005 Phase speed and attenuation in bubbly liquids inferred from impedance measurements near the individual bubble resonance frequency. *J. Acoust. Soc. Am.* **117**, 1895–1910. (doi:10.1121/1.1859091)

Yim, G. T. & Leighton, T. G. 2010 Real-time on-line monitoring of ceramic 'slip' in pottery pipe-lines using ultrasound. *Ultrasonics* **50**, 60–67. (doi:10.1016/j.ultras.2009.07.008)